

## Temperature Inhomogeneity during Multibubble Sonoluminescence\*\*

Hangxun Xu, Nick G. Glumac, and Kenneth S. Suslick\*

When a liquid is subjected to high-intensity ultrasound, bubbles are formed, grow, and implodingly collapse. This phenomenon of acoustic cavitation generates both chemical reactions (i.e., sonochemistry) and the emission of light (i.e., sonoluminescence, SL).<sup>[1-7]</sup> It is generally agreed that both sonochemistry and sonoluminescence result from the intense compressional heating of gas and vapor inside the collapsing bubbles, and the extraordinary temperatures and pressures thus created.<sup>[4]</sup> The emission of light can occur either from a cloud of cavitating bubbles (i.e., multibubble sonoluminescence, MBSL), or in a carefully controlled standing wave acoustic field from a single isolated bubble (i.e., single-bubble sonoluminescence, SBSL). MBSL is more closely related to sonochemistry, and quantification of the conditions generated during MBSL can lead to a better understanding of sonochemistry. Measurement of atomic and molecular emission from volatile species during MBSL revealed effective temperatures of thousands of Kelvins created during bubble collapse.<sup>[8,9]</sup> Little is known, however, about the origin of emission derived from nonvolatile species during MBSL. This emission is directly relevant to the observed sonochemistry of dissolved reactants.

Extensive emission bands and lines have been observed both from aqueous and non-aqueous liquids during MBSL,<sup>[8-14]</sup> and can be used as spectroscopic thermometers to quantify the conditions generated inside the collapsing bubbles. For example, the Swan bands of C<sub>2</sub>,<sup>[8,14]</sup> excited-state metal atoms (e.g., Fe, Cr, Mo),<sup>[9]</sup> and even excited state Ar emission<sup>[13]</sup> have been used to measure the intracavity temperatures. Other nonspectroscopic methods have also been used to measure the temperatures of cavitating bubbles.<sup>[15-19]</sup> No prior study, however, has reported simultaneous measurement of temperature from two or more independent emitting species, which would permit one to probe the homogeneity of the temperature profile generated in bubble clouds from spatial variance during acoustic cavitation. By examining the MBSL from aqueous H<sub>3</sub>PO<sub>4</sub> solutions, we have observed ultrabright sonoluminescence, found strong molec-

ular emissions from both OH· and PO· radicals, and have succeeded in using both simultaneously as spectroscopic thermometers. There is a dramatic temperature inhomogeneity that is dependent on the location within the bubble cloud and is consistent with two distinct kinds of cavitating bubbles: those that collapse symmetrically and those that do not.

H<sub>3</sub>PO<sub>4</sub> is a strongly hydrogen-bonded liquid; it has a relatively high viscosity and low vapor pressure (ca. 2.4 Torr for 85 % H<sub>3</sub>PO<sub>4</sub>). Interestingly, the vapor of H<sub>3</sub>PO<sub>4</sub> consists of water molecules alone; there are no acid molecules present in the vapor over most concentrated H<sub>3</sub>PO<sub>4</sub> samples, even at high temperatures.<sup>[20]</sup> Thus, in the gas phase of H<sub>3</sub>PO<sub>4</sub>, the only volatile component inside the bubbles is water vapor; the phosphoric acid molecules can be considered as nonvolatile species during MBSL.<sup>[21]</sup> Ultrabright sonoluminescence from 85 % H<sub>3</sub>PO<sub>4</sub> saturated with noble gases can be observed by naked eye, even in a well-lit room, as shown in Figure 1.

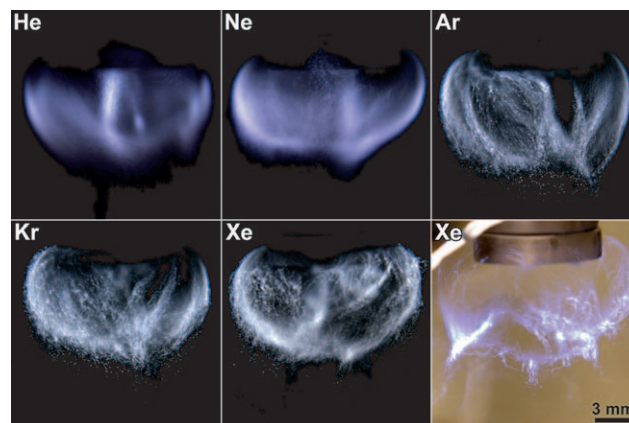


**Figure 1.** Photographs of ultrabright sonoluminescence from 85 % H<sub>3</sub>PO<sub>4</sub> saturated with He, Ne, Ar, Kr, and Xe. To optimize the images, different exposure times were used for each gas: He 20 s, Ne 10 s, Ar 0.5 s, Kr 0.25 s, Xe in dark 0.25 s, and Xe in room light 0.17 s. The light from Xe-saturated H<sub>3</sub>PO<sub>4</sub> is comparable in brightness to the fluorescent room lighting, which is seen as a reflection on the outside of the quartz flask of the lower right panel. Sonication conducted at 20 kHz, 17 W cm<sup>-2</sup>, with a 1 cm<sup>2</sup> Ti horn directly immersed in the solution at 298 K.

MBSL from 85 % H<sub>3</sub>PO<sub>4</sub> is much brighter compared to the light emitted during MBSL in water<sup>[22]</sup> and even brighter than MBSL<sup>[13]</sup> in 95 % sulfuric acid. A semiquantitative comparison (see also Figure S1 in the Supporting Information) of MBSL intensity is possible: the observed luminosities relative to phosphoric acid are less than 0.25 % in water and 65 % in sulfuric acid.

[\*] H. Xu, Prof. K. S. Suslick  
School of Chemical Sciences  
University of Illinois at Urbana-Champaign  
Urbana, IL 61801 (USA)  
Fax: (+1) 217-244-3186  
E-mail: ksuslick@uiuc.edu  
Homepage: <http://www.scs.uiuc.edu/suslick>  
Prof. N. G. Glumac  
Department of Mechanical Science and Engineering  
University of Illinois at Urbana-Champaign  
Urbana, IL 61801 (USA)

[\*\*] This work is supported by the National Science Foundation.

Supporting information for this article is available on the WWW under <http://dx.doi.org/10.1002/anie.200905754>.

The origin of the MBSL from 85%  $\text{H}_3\text{PO}_4$  emission depends on the dissolved inert gas. Under He or Ne, the MBSL spectra show strong molecular emission from  $\text{OH}^\bullet$  ( $\text{A}^2\Sigma^+-\text{X}^2\Pi$ ) and the  $\text{PO}^\bullet$   $\beta$  system ( $\text{B}^2\Sigma^+-\text{X}^2\Pi$ ), with bands at 310 nm and 325 nm respectively<sup>[23]</sup> (Figure S2 in the Supporting Information). Under He, one also observes the  $\text{PO}^\bullet$   $\gamma$  system ( $\text{A}^2\Sigma^+-\text{X}^2\Pi$ ) emission, which is frequently observed in flames containing phosphorus<sup>[23]</sup> (Figure S3 in the Supporting Information). The  $\text{OH}^\bullet$  and  $\text{PO}^\bullet$  molecular emission bands are monotonically broadened as the dissolved gas goes from He to Ne to Ar to Kr to Xe (Figure S2 in the Supporting Information). With Kr and Xe, the molecular emission bands are broadened completely. Given the higher expected cavitation temperatures with the heavier inert gases (arising from decreased thermal conductivity), the broadening of the molecular emission is consistent with expected dissociation of the  $\text{OH}^\bullet$  and  $\text{PO}^\bullet$  radicals.

Excited  $\text{OH}^\bullet$  radicals are also observed during MBSL in aqueous solutions,<sup>[12,24]</sup> but their emission is too weak and too broad to be used for spectroscopic thermometry. In contrast, the MBSL in 85%  $\text{H}_3\text{PO}_4$  under He shows very strong  $\text{OH}^\bullet$  and  $\text{PO}^\bullet$  emission and excellent resolution of the emission fine structure. As shown in Figure 2, we are able to easily observe  $\text{OH}^\bullet$   $\text{A}^2\Sigma^+-\text{X}^2\Pi$  rovibronic bands (305–315 nm) together with  $\text{PO}^\bullet$   $\text{B}^2\Sigma^+-\text{X}^2\Pi$  transitions (320–340 nm). We can see that the  $\text{PO}^\bullet$  emission decreases rapidly below 320 nm and hence does not affect the accuracy of the measurement of  $\text{OH}^\bullet$  emission. This property permits us to use spectroscopic methods to measure emission temperatures from two independent emission species.

Calculated  $\text{OH}^\bullet$  emission spectra can be generated from LIFBASE, a database and spectral simulation program for diatomic molecules that has been extensively used to determine emission temperatures from excited diatomic molecules in flames and laser-induced fluorescence.<sup>[25]</sup> By fitting our experimental spectra for  $\text{OH}^\bullet$  emission with calculated spectra yields an effective emission temperature of  $(9500 \pm 300)$  K (Figure 2b). This temperature is significantly higher than that observed from pure water (ca. 5000 K),<sup>[14,26]</sup> which is as expected from the significant difference in the vapor pressure of water (24 torr) and 85%  $\text{H}_3\text{PO}_4$  (2.4 Torr): less of the compressional energy during cavitation is consumed by polyatomic vibrations, rotations, and especially endothermic bond dissociation.<sup>[27]</sup>

The emission from excited  $\text{PO}^\bullet$  radicals can also be used as a spectroscopic thermometer to probe the intracavity temperatures generated during MBSL. The  $\beta$  system of  $\text{PO}^\bullet$  emission in the 320–340 nm wavelength range has been extensively studied.<sup>[23]</sup> We can use the identical approach applied in LIFBASE to calculate  $\text{PO}^\bullet$  emission spectra using known spectroscopic constants<sup>[28]</sup> and calculated Franck–Condon factors.<sup>[29]</sup> Because the  $\text{OH}^\bullet$  emission tail at approximately 330 nm overlaps the  $\text{PO}^\bullet$  emission band, we subtract the  $\text{OH}^\bullet$  emission (as generated from LIFBASE) from the observed MBSL spectrum to obtain an accurate  $\text{PO}^\bullet$  emission spectrum. By fitting the  $\text{PO}^\bullet$  emission spectra (Figure 2c), the emission temperature of  $\text{PO}^\bullet$  is determined to be  $(4000 \pm 400)$  K, which is substantially lower than that measured from the  $\text{OH}^\bullet$  emission ( $(9500 \pm 300)$  K). Similar results are

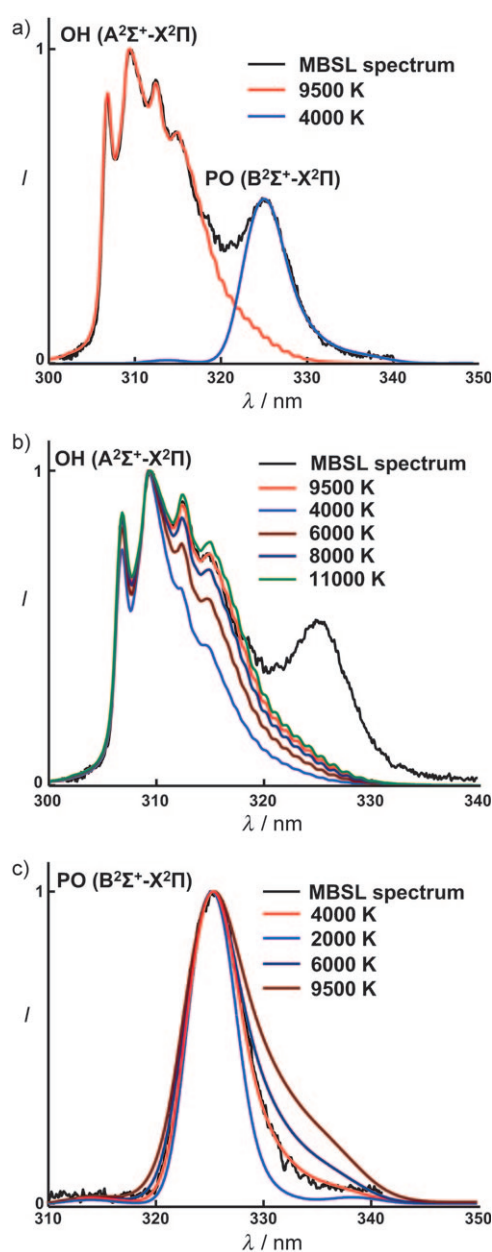


**Figure 2.** a) Spectrum of  $\text{OH}^\bullet$  ( $\text{A}^2\Sigma^+-\text{X}^2\Pi$ ) and  $\text{PO}^\bullet$  ( $\text{B}^2\Sigma^+-\text{X}^2\Pi$ ) emission from MBSL in 85%  $\text{H}_3\text{PO}_4$  saturated with He and irradiated with ultrasound compared to the best fit calculated spectra (red: calculated  $\text{OH}^\bullet$  emission spectrum at 9500 K; blue: calculated  $\text{PO}^\bullet$  emission spectrum at 4000 K). b) observed MBSL  $\text{OH}^\bullet$  emission spectrum compared to calculated  $\text{OH}^\bullet$  emission spectra at different temperatures. c) Observed MBSL  $\text{PO}^\bullet$  emission spectrum compared to calculated  $\text{PO}^\bullet$  emission spectra at different temperatures. Sonication was conducted at 20 kHz and  $17 \text{ W cm}^{-2}$  with a Ti horn directly immersed in the solution at 298 K. The calculated spectra assumed thermal equilibrium and a Lorentzian profile. The underlying continuum has been subtracted; spectra are normalized to the maximum intensity peak.

also observed at higher acoustic intensity (Figure S4 in the Supporting Information).

At first glance, the different MBSL temperatures from the two simultaneously observed, independent molecular species are paradoxical because both  $\text{OH}^\bullet$  and  $\text{PO}^\bullet$  emissions are from

same cavitation event. The observed temperature inhomogeneity can, however, be explained by the two different cavitating bubble populations that involve nonvolatile species, as recently observed<sup>[30–32]</sup> during MBSL in  $\text{H}_2\text{SO}_4$  and  $\text{H}_3\text{PO}_4$ . We recently demonstrated<sup>[30]</sup> by doping  $\text{H}_3\text{PO}_4$  with  $\text{Na}_3\text{PO}_4$  that there are two distinct cavitating bubble populations in  $\text{H}_3\text{PO}_4$ : 1) stationary bubbles whose collapse is highly symmetric and 2) rapidly moving bubbles whose collapse is much less symmetric and associated injection of liquid nanodroplets into the gas phase of the collapsing bubbles. The  $\text{OH}^\bullet$  emission comes predominantly from the first class of collapsing bubbles. In contrast, the  $\text{PO}^\bullet$  radical, which is a decomposition product of nonvolatile  $\text{H}_3\text{PO}_4$ , is analogous to the emission of alkali metal atoms in aqueous solution and represents the conditions present in the second class of cavitating bubbles.

Consistent with this interpretation, we also observe spatial separation of the cavitating bubble populations. As shown in Figure 3a, there are two different bubble populations:  $\text{OH}^\bullet$  emission appears both at the top and bottom of the cavitating bubble cloud, whereas  $\text{PO}^\bullet$  emission is only observable at the bottom of the cloud.  $\text{PO}^\bullet$  emission originates from nonvolatile molecules and involves injection of liquid phosphoric acid droplets into the interior of bubbles by capillary wave action, microjetting, or bubble coalescence because of the significant

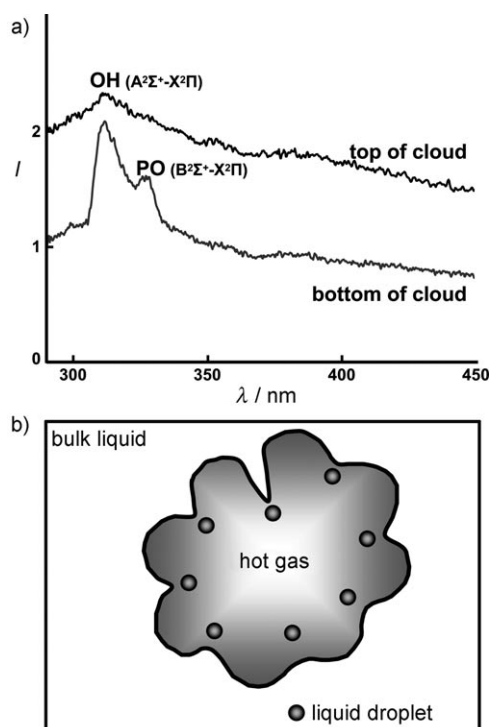


**Figure 3.** a) MBSL spectra taken at the top and bottom of the cavitating bubble cloud from 85%  $\text{H}_3\text{PO}_4$  saturated with He.  $\text{OH}^\bullet$  emission is observable both at the top and bottom of the cavitating bubble cloud, but  $\text{PO}^\bullet$  emission only appears at the bottom of the cavitating bubble cloud where nonsymmetric bubble collapse occurs. Sonication conducted at 20 kHz,  $25 \text{ W cm}^{-2}$ , with a  $1 \text{ cm}^2$  Ti horn directly immersed in the solution at 298 K. b) A schematic representation of the nonsymmetric collapse of bubbles that injects liquid nanodroplets into the hot gas phase of the collapsing bubbles.

deformation during bubble collapse in the dense cloud of cavitating bubbles,<sup>[30,33–36]</sup> as shown in Figure 3b. Once the droplets enter the hot interior of the bubble, the solvent evaporates and decomposition of  $\text{H}_3\text{PO}_4$  molecules analogous to the processes that occurs in flames begins, and generates excited  $\text{PO}^\bullet$  radicals. The evaporation of the solvent in the liquid droplet and endothermic decomposition of  $\text{H}_3\text{PO}_4$  and  $\text{H}_2\text{O}$  molecules consume a great amount of cavitation energy. Thus, liquid droplets can cool down hot spots inside the cavitating bubbles that contain liquid droplets. The measured  $\text{PO}^\bullet$  emission temperature represents the hot-spot conditions inside nonsymmetrically collapsing bubbles that contain liquid droplets, and is much lower than the measured  $\text{OH}^\bullet$  emission temperature that dominantly represents the more symmetric collapsing bubbles. Presumably, the spatial separation of the two bubble populations is caused by the pressure gradient propagated from the ultrasonic horn; one might not observe such separation in a more uniform ultrasonic field.

The dissociation energy of diatomic molecules provides an upper temperature limit to their usefulness for spectroscopic thermometry: at a sufficiently high temperature, the emitting diatomic would dissociate within the emission timeframe.<sup>[37,38]</sup> The dissociation energies of  $\text{OH}^\bullet$  and  $\text{PO}^\bullet$  are  $428 \text{ kJ mol}^{-1}$  and  $595 \text{ kJ mol}^{-1}$ , respectively.<sup>[39]</sup> In flame spectroscopy, the temperature measured from  $\text{OH}^\bullet$  emission can be up to 10000 K.<sup>[38]</sup> Excited  $\text{PO}^\bullet$  radicals dissociate at even higher temperatures and are frequently observed in the presence of a phosphorous source from very high temperature arcs, flames, and discharges. Thus, for our studies, spectroscopic thermometry using  $\text{OH}^\bullet$  and  $\text{PO}^\bullet$  radicals is valid because both species will persist even under the extreme intracavity conditions that we observe.

In conclusion, spectroscopic methods have become a formidable method for quantifying the temperatures generated during cavitation.<sup>[4,8,9,13,14]</sup> We have reported the application of this approach by using two independent molecular thermometers ( $\text{OH}^\bullet$  and  $\text{PO}^\bullet$  molecular emission) inside a cavitating cloud of bubbles during MBSL. We find that there are two distinct cavitating bubble populations in  $\text{H}_3\text{PO}_4$  and observe spatial separation of the emission spectra from 1) bubbles whose collapse is highly symmetric near the ultrasonic horn and 2) rapidly moving bubbles whose collapse is much less symmetric and associated injection of liquid nanodroplets into the gas phase of the collapsing bubbles. The spectroscopic temperatures from  $\text{OH}^\bullet$  emission comes dominantly from very hot bubbles (ca. 9500 K) that collapse near the ultrasonic horn without injection of droplets, whereas the  $\text{PO}^\bullet$  emission comes from colder (ca. 4000 K) bubbles that collapse nonsymmetrically far from the horn.

### Experimental Section

The experimental apparatus used here is similar to that previously reported.<sup>[13,30]</sup> Ultrasonic irradiation was performed using a Sonics and Materials VCX 600 Vibra Cell at 20 kHz with a 1 cm diameter Ti horn immersed in  $\text{H}_3\text{PO}_4$  (85 wt %) in a quartz round bottom flask (ca. 100 mL) after sparging the thoroughly deaerated liquid with the desired noble gas (He, Ne, Ar, Kr, or Xe) at around 298 K. The low-resolution MBSL measurements were made with an 0.32 m monochromator equipped with a  $300 \text{ gr mm}^{-1}$  grating blazed at 250 nm and

fitted with a 1024×256 pixel liquid nitrogen cooled CCD camera. High-resolution MBSL spectra were acquired with a 1200 gr mm<sup>-1</sup> grating blazed at 330 nm, and each spectrum was averaged from fifteen spectra each collected for 80 s. The best-fit calculated spectra for OH<sup>•</sup> emission simulation were generated with the LIFBASE program.<sup>[25]</sup> The emission spectra of a β system of PO<sup>•</sup> were modeled using the identical approach implemented in LIFBASE but using known spectroscopic constants<sup>[28]</sup> and calculated Franck–Condon factors.<sup>[29]</sup>

Received: October 13, 2009

Published online: January 4, 2010

**Keywords:** luminescence · radicals · sonochemistry · sonoluminescence · ultrasound

- 
- [1] K. S. Suslick in *Sonochemistry: Its Chemical, Physical and Biological Effects* (Ed.: K. S. Suslick), VCH Publishers, New York, **1988**.
- [2] J. L. Luche, C. Bianchi, *Synthetic Organic Sonochemistry*, Plenum, New York, **1998**.
- [3] T. J. Mason, J. P. Lorimer, *Applied Sonochemistry: The Uses of Power Ultrasound in Chemistry and Processing*, Wiley-VCH, Weinheim, **2002**.
- [4] K. S. Suslick, D. J. Flannigan, *Annu. Rev. Phys. Chem.* **2008**, *59*, 659.
- [5] M. P. Brenner, S. Hilgenfeldt, D. Lohse, *Rev. Mod. Phys.* **2002**, *74*, 425.
- [6] M. Ashokkumar, F. Grieser, *ChemPhysChem* **2004**, *5*, 439.
- [7] S. J. Putterman, K. R. Weninger, *Annu. Rev. Fluid Mech.* **2000**, *32*, 445.
- [8] E. B. Flint, K. S. Suslick, *Science* **1991**, *253*, 1397.
- [9] W. B. McNamara, Y. T. Didenko, K. S. Suslick, *Nature* **1999**, *401*, 772.
- [10] K. S. Suslick, E. B. Flint, *Nature* **1987**, *330*, 553.
- [11] E. B. Flint, K. S. Suslick, *J. Am. Chem. Soc.* **1989**, *111*, 6987.
- [12] Y. T. Didenko, S. P. Pugach, *J. Phys. Chem.* **1994**, *98*, 9742.
- [13] N. C. Eddingsaas, K. S. Suslick, *J. Am. Chem. Soc.* **2007**, *129*, 3838.
- [14] Y. T. Didenko, W. B. McNamara, K. S. Suslick, *J. Am. Chem. Soc.* **1999**, *121*, 5817.
- [15] K. S. Suslick, R. E. Cline, Jr., D. A. Hammerton, *J. Am. Chem. Soc.* **1986**, *108*, 5641.
- [16] V. Misik, N. Miyoshi, P. Riesz, *J. Phys. Chem.* **1995**, *99*, 3605.
- [17] A. J. Colussi, L. K. Weavers, M. R. Hoffman, *J. Phys. Chem. A* **1998**, *102*, 6927.
- [18] M. Ashokkumar, F. Grieser, *J. Am. Chem. Soc.* **2005**, *127*, 5326.
- [19] P. M. Kanthale, M. Ashokkumar, F. Grieser, *J. Phys. Chem. C* **2007**, *111*, 18461.
- [20] B. J. Fontana, *J. Am. Chem. Soc.* **1951**, *73*, 3348.
- [21] A. Chakravarty, T. Georghiou, T. E. Phillipson, A. J. Walton, *Phys. Rev. E* **2004**, *69*, 066317.
- [22] T. Lepoint, F. Lepoint-Mullie, S. Labouret, J. M. Leveque, C. Petrier, D. Krefting, R. Geisler, R. Mettin, T. Kurz, W. Lauterborn, *5th World Congress on Ultrasonics*, Paris, **2003**, p. 955.
- [23] R. W. B. Pearse, A. G. Gaydon, *The Identification of Molecular Spectra*, 4th ed., Chapman and Hall, London, **1976**.
- [24] T. Lepoint, F. Lepoint-Mullie, N. Voglet, S. Labouret, C. Pétrier, R. Avni, J. Luque, *Ultrason. Sonochem.* **2003**, *10*, 167.
- [25] J. Luque, D. R. Crosley, “LIFBASE, Database and Spectral Simulation for Diatomic Molecules (v. 2.0.60)”, Report MP-99-009; SRI International, **1999**.
- [26] Y. T. Didenko, W. B. McNamara, K. S. Suslick, *J. Phys. Chem. A* **1999**, *103*, 10783.
- [27] Y. T. Didenko, K. S. Suslick, *Nature* **2002**, *418*, 394.
- [28] K. Huber, G. Herzberg, *Constants of Diatomic Molecules*, 1st ed., Van Nostrand, New York, **1979**.
- [29] K. C. Smyth, W. G. Mallard, *J. Chem. Phys.* **1982**, *77*, 1779.
- [30] H. X. Xu, N. C. Eddingsaas, K. S. Suslick, *J. Am. Chem. Soc.* **2009**, *131*, 6060.
- [31] S. Hatanaka, S. Hayashi, S. Abe, P. K. Choi, *AIP Conf. Proc.* **2008**, *1022*, 205.
- [32] D. Sunartio, K. Yasui, T. Tuziuti, T. Kozuka, Y. Iida, M. Ashokkumar, F. Grieser, *ChemPhysChem* **2007**, *8*, 2331.
- [33] H. Yuan, A. Prosperetti, *Phys. Fluids* **1997**, *9*, 127.
- [34] S. T. Thoroddsen, T. G. Etoh, K. Takehara, *Annu. Rev. Fluid Mech.* **2008**, *40*, 257.
- [35] A. J. Colussi, H. M. Hung, M. R. Hoffman, *J. Phys. Chem. A* **1999**, *103*, 2696.
- [36] T. Tuziuti, K. Yasui, Y. Iida, A. Sivakumar, *Res. Chem. Intermed.* **2004**, *30*, 755.
- [37] L. S. Bernstein, M. R. Zakin, E. B. Flint, K. S. Suslick, *J. Phys. Chem.* **1996**, *100*, 6612.
- [38] A. G. Gaydon, *The Spectroscopy of Flames*, 2nd ed., Chapman and Hall, London, **1974**.
- [39] B. deB. Darwent, *Bond Dissociation Energies in Simple Molecules*, NSRDS-NBS 31, (US GPO, Washington DC, 1970); <http://www.nist.gov/srd/nsrds/NSRDS-NBS31.pdf>.
-